Sustainable Energy & Fuels

Cobalt Porphyrin Intercalation into Zirconium Phosphate Layers for Electrochemical Water Oxidation

Journal:	*Sustainable Energy & Fuels*
Manuscript ID	SE-ART-07-2020-001134.R1
Article Type:	Paper
Date Submitted by the Author:	06-Oct-2020
Complete List of Authors:	Barraza Alvarez, Isabel; University of Texas at El Paso, Department of Chemistry and Biochemistry Wu, Yanyu; University of Texas at El Paso, Department of Chemistry Sanchez, Joel; Stanford University, Chemical Engineering Ge, Yulu; University of Texas at El Paso, Department of Chemistry and Biochemistry Ramos Garces, Mario; Universidad de Puerto Rico Recinto de Rio Piedras Chu, Tong; University of Texas at El Paso, Department of Chemistry and Biochemistry Jaramillo, Thomas; Stanford University, Assistant Professor of Chemical Engineering Colón, Jorge; University of Puerto Rico, Chemistry Villagran, Dino; University of Texas at El Paso, Department of Chemistry and Biochemistry

ARTICLE

Cobalt Porphyrin Intercalation into Zirconium Phosphate Layers for Electrochemical Water Oxidation

Received 00th January 20xx,
Accepted 00th January 20xx

DOI: 10.1039/x0xx00000x

Isabel Barraza Alvarez,[a‡] Yanyu Wu,[a‡] Joel Sanchez,[b] Yulu Ge,[a] Mario V. Ramos-Garcés,[c] Tong Chu,[a,d] Thomas F. Jaramillo,[b] Jorge L. Colón,[c] and Dino Villagrán*[a]

A cobalt porphyrin molecule, namely CoTcPP (TcPP = the dianion of meso-tetra(4-carboxyphenyl)porphyrin), is intercalated into zirconium phosphate (ZrP) layers as an effective way to heterogenize a porphyrin-based molecular electrocatalyst. Fourier-transform infrared (FT-IR) spectroscopy, X-ray powder diffraction (XRPD) measurements, UV-Vis spectroscopy, elemental mapping, energy dispersive X-ray (EDX) analysis, inductively coupled plasma mass spectrometry (ICP-MS) and X-ray photoelectron spectroscopy (XPS) were utilized to determine the successful intercalation of CoTcPP into ZrP. While the CoTcPP molecule is not amendable to be used as a heterogeneous catalyst in basic environment due to the carboxylic groups, the intercalated species (CoTcPP/ZrP) is effective towards water oxidation from KOH aqueous solution when ulitized as a heterogeneous electrocatalyst and shows remarkable catalytic durability. Electrochemical results show that CoTcPP/ZrP requires an overpotential of 0.467 V to achieve a current density of 10 mA/cm^2 while the pristine α-ZrP shows negligible electrocatalytic OER behavior.

INTRODUCTION

Development of renewable energy technologies requires efficient and cost-effective approaches for energy storage.[1] A prevailing strategy is to store energy in chemical bonds.[2] For instance, the hydrogen-hydrogen bond in H_2 is a promising medium due to its high gravimetric energy density and that its combustion only yields water as the byproduct.[3,4] Therefore, the production of hydrogen gas through water electrolysis has garnered much attention as a promising alternative to generate clean fuels.[5] Water electrolysis proceeds via two separate half reactions, which correspond to the hydrogen evolution reaction (HER) and oxygen evolution reaction (OER).[6] Splitting water to generate hydrogen and oxygen gases is a thermodynamically and kinetically challenging process with a ΔG of +237 kJ mol^{-1} and a high overpotential requirement due to the formation of high-energy intermediates.[6,7] More particularly, most of the energy inefficiency from water electrolysis originates from the OER process because it requires the transfer of four electrons and four protons.[8,9] Thus, improving the OER kinetics is highly desirable to lower the overall driving overpotential of water splitting to generate hydrogen and oxygen gases.[10] So far, the lack of cost-effective, efficient and robust electrocatalysts is considered to be one of the challenges of studying the OER, which has stimulated the exploration of a variety of catalytic systems with enhanced performance.

Metalloporphyrins have been well established as HER and OER electrocatalysts through both experimental and theoretical studies.[11–17] Particularly, several recent reports demonstrated the use of transition-metal porphyrin molecular catalysts for electrochemical oxygen production. Cao el.al reported a water-soluble copper porphyrin that can produce oxygen gas from neutral aqueous environment with low overpotential of 310 mV at current density of 0.10 mA/cm^{-2} from a homogeneous system.[18] Another recent work shown by Wan and coworkers shows CoTPP (TPP = dianion of 5,10,15,20-tetraphenylporphyrin) as an electrocatalyst for OER from basic aqueous solutions and studied its catalytic mechanism.[19] While metalloporphyrins are mostly treated as homogeneous electrocatalysts where they are useful for elucidating mechanistic insights, their efficiencies are hampered by the limited number of active catalytic sites in contact with the electrodes and substrates.[20] Thus, much progress has been made to investigate metalloporphyrin-based heterogeneous catalytic systems to improve the catalytic efficiency and for easier recovery and recyclability of the catalysts.[21] Metalloporphyrin-based heterogeneous catalysts have been successfully developed through the construction of insoluble organic polymers,[21–23] grafting the molecular catalysts directly onto the electrode materials[24,25] and immobilizing the metalloporphyrins using catalyst supports,[26–28] among other methods.[29,30]

Zirconium phosphate (ZrP) is a type of inorganic crystalline layered nanomaterial.[31,32] Recently, two ZrP phases have

[a] Department of Chemistry and Biochemistry, The University of Texas at El Paso, El Paso, TX 79968, USA. E-mail: dino@utep.edu
[b] Department of Chemical Engineering, Stanford University, Stanford, CA 94305, USA
[c] Department of Chemistry, University of Puerto Rico at Río Piedras, 17 Ave. Universidad STE 1701, San Juan, PR 00925-2537, USA
[d] Department of Chemistry, Beijing Normal University, Beijing 100875, China
‡Isabel Barraza Alvarez and ‡Yanyu Wu contributed equally

Electronic Supplementary Information (ESI) available: ^{1}H NMR and UV-Vis spectrum of H_2TcPP, EDX spectrum, SEM images and the corresponding elemental maps of α-ZrP and CoTcPP/ZrP are included in Supporting Information.

received much attention: zirconium bis(monohydrogen orthophosphate) monohydrate [$Zr(HPO_4)_2{\cdot}H2O$, α-ZrP] and zirconium bis(monohydrogen orthophosphate) hexahydrate [$Zr(HPO_4)_2{\cdot}6H_2O$, θ-ZrP].[33,34] Besides the difference in the number of water molecules per formula unit of these two phases of ZrP, α-ZrP and θ-ZrP have an interlayer distance of 7.6 Å and 10.4 Å, respectively.[35] Due to its interesting layered structure and its ability of intercalation and ion-exchange, ZrP is regarded as a promising supporting platform for encapsulating ionic metals, molecules, metal oxides and even polymers, which result in a wide range of applications including, but not limited to catalysis, drug delivery and photochemical studies.[31,36–39] While α-ZrP is suited for the intercalation of small cations (those smaller than 2.61 Å), θ-ZrP is more favorable when larger cations and molecular complexes are being intercalated.[35,40] Previous work has described the use of both layered ZrP and exfoliated ZrP as the catalyst support for different late transition-metal cations (Fe^{3+}, Fe^{2+}, Co^{2+} and Ni^{2+}). These cation-exchanged ZrP materials were assessed as electrocatalysts for water oxidation and demonstrate promising catalytic activity.[36,41–43] In addition to transition cations, ZrP is known to be able to immobilize a variety of molecules.[35,40,44] Combined with our interest in both metalloporphyrins as effective electrocatalysts and ZrP as a layered material, in this work we investigate the use of ZrP to intercalate metalloporphyrin molecules as means to heterogenize molecular electrocatalysts. Herein, we present the intercalation of a cobalt porphyrin molecule CoTcPP [TcPP = the dianion of meso-tetra(4-carboxyphenyl)porphyrin] into ZrP layers as a heterogeneous OER electrocatalyst. We report the synthesis and chemical characterization of this CoTcPP-intercalated ZrP, including XPS, XRPD, FT-IR, ICP-MS, UV-Vis, EDX, and SEM, and the evaluation of both intercalated and pristine ZrP as electrocatalysts for oxygen production by means of electrochemical measurements. We show that the CoTcPP molecule can be effectively embedded inside the ZrP layers while maintaining the metalloporphyrin molecular structure. This immobilized material is catalytically active towards water oxidation to produce oxygen gas with a modest overpotential of 0.476 V at a selected current density of 10 mA/cm^2 when evaluated as a heterogeneous catalyst. This material also exhibits remarkable durability under oxidation condition in strong basic media.

EXPERIMENTAL SECTION

Materials. All materials used were obtained from commercially available sources. Pyrrole (C_4H_5N), 4-carboxybenzaldehyde ($C_8H_6O_3$), zirconium (IV) oxychloride octahydrate ($ZrOCl_2 \cdot 8H_2O$), *p*-chloranil ($C_6Cl_4O_2$), boron trifluoride diethyl etherate ($C_4H_{10}BF_3O$) and Nafion®117 (5%) were purchased from Sigma Aldrich and cobalt acetate tetrahydrate [$Co(OAC)_2{\cdot}4H_2O$] was purchased from Strem Chemicals. Sulfuric acid (H_2SO_4), phosphoric acid (H_3PO_4), propionic acid ($C_3H_6O_2$), ethanol (C_2H_6O), methanol (CH_4O) and dimethylformamide (C_3H_7NO) were obtained from Fisher Scientific. Carbon black (Vulcan XC-72) was purchased from Fuel Cell Store. Pyrrole was freshly distilled and $Co(OAC)_2{\cdot}4H_2O$ was vacuumed dried at 80 °C before being used. All other chemicals were used as received. θ-ZrP and CoTcPP were synthesized using previously reported methods.

Physical and chemical measurements. ^{1}H NMR spectra were obtained using a Bruker 400 MHz NMR spectrometer. UV-Vis spectra were recorded on a SEC2000 spectra system equipped with a VISUAL SPECTRA 2.1 software. Fourier-transform infrared (FT-IR) spectroscopy was performed on an Agilent Cary 630 FT-IR spectrometer with an attenuated total reflectance (ATR) accessory. X-ray powder diffraction (XRPD) was recorded on a Bruker D8 Discovery X-ray diffractometer with Cu Kα radiation source (λ = 1.5406 Å). The spacing distance was calculated according to Bragg's law ($n\lambda = 2d_{hkl} \sin\theta$), where λ is the wavelength of the X-ray source used, n is a positive integer, d_{hkl} is the interlayer distance between the crystallographic planes (*h*, *k*, *l*) in the unit cell, and θ is the diffraction angle obtained from the XRPD patterns. Scanning electron microscopy (SEM), elemental mapping and energy dispersive X-ray (EDX) spectroscopy were analyzed on a Hitachi S-4800 instrument equipped with an EDX microanalysis system. X-ray photoelectron spectroscopy (XPS) analysis was carried out on a Physical Electronics PHI 5000 VersaProbe with an Al Kα source, where all the spectra were calibrated to the carbon 1s peak at 284.8 eV and fitted using a Shirley background. The atomic concentration of Co of the as-prepared samples were obtained through inductively coupled plasma mass-spectrometry (Thermo Scientific, XSERIES 2 ICP-MS). The samples were digested in an aqua regia matrix before analysis. All calibration standards were TraceCERT® certified and obtained from Sigma-Aldrich.

Synthesis of θ-Zirconium Phosphate (θ-ZrP) nanomaterial. The synthesis of θ-ZrP was performed following a previously described procedure.[45] A solution containing 100 mL 6.0 M H_3PO_4 was heated at 94 °C. While stirring, 100 mL of 0.05 M $ZrOCl_2{\cdot}8H_2O$ in aqueous solution was added dropwise and the reaction mixture was allowed to stir at 94 °C for 2 days. Afterwards, the resultant suspension was centrifuged and the remaining precipitate was washed with deionized water. The α-ZrP control material was obtained upon dehydration of θ-ZrP under vacuum.

Synthesis of meso-tetra(4-carboxyphenyl)porphyrin (H_2TcPP).[46] 4-carboxybenzaldehyde (5.00 g, 33.30 mmol) and pyrrole (2.23 g, 33.30 mmol) were refluxed in propionic acid (500 mL) for 2 hours with constant stirring. Then to the reaction mixture was added 100 mL of methanol and allowed to cool down. Afterwards the crude product was filtered using a medium coarse filter frit and washed with warm water. The final product was dried under vacuum at 80 °C. (Yield: 3.0 g, 45%) ^{1}H NMR (d_6-DMSO) δ: 13.29 ppm (s, 4H), 8.86 ppm (s, 8H), 8.35 ppm (m, 16H), –2.95 ppm (s, 2H); UV-Vis (EtOH): λ_{max}: 419, 519, 552, 592, 648 nm.

Synthesis of cobalt meso-tetra(4-carboxyphenyl)porphyrin (CoTcPP).[46] A mixture of H_2TcPP (0.100 g, 0.126 mmol) and anhydrous $Co(OAC)_2$ (0.0266 g, 0.150 mmol) in DMF (20 mL) was reacted under reflux for an hour. Then, the reaction was allowed to cool down and the crude material was filtered. The filter cake was washed with deionized water and vacuum dried at 80 °C. (Yield: 0.078 g, 73%) UV-Vis (EtOH): λ_{max}: 429, 546 nm.

Synthesis of CoTcPP-modified ZrP material (CoTcPP/ZrP). A mixture of CoTcPP (0.0600 g, 0.0702 mmol) and θ-ZrP (0.0270 g, 0.0702 mmol) in ethanol (500 mL) was stirred under room temperature for 5 days. The solution was then centrifuged and the precipitate was collected and washed with ethanol.

Electrochemical Methods. All of the electrochemical measurements were carried out using a three-electrode electrochemical cell with a catalyst-modified glassy carbon rotating disk electrode, an Ag/AgCl reference and a Pt wire counter electrode. All cyclic voltammetry studies were performed in 0.1 M KOH electrolyte solutions constantly bubbled with oxygen gas with a scan rate of 10 mV/s. The working electrode was constantly rotated at 1600 RPM. Ohmic correction was performed after each measurement and the resistance of the electrolyte solution was obtained at 100 kHz. Electrochemical impedance spectroscopy (EIS) was obtained at an overpotential (η) of 0.250 V from 100 kHz to 0.1 Hz with an AC voltage of 5 mV.

Bulk electrolysis was performed in a gas-tight two-compartment H-shaped electrochemical cell separated by a frit. One part of the cell consists of the working electrode and the reference electrode while the other one contains the counter electrode. Both compartments of the cell were purged with argon gas prior to the electrochemical study to preclude oxygen gas. Gas detection and quantitative analysis were performed by a SHIMADZU GC-8A gas chromatograph (GC) subsequently after bulk electrolysis. Faradaic efficiency was obtained using the equation below:

Faradaic efficiency (%) = [96485 C/mol × 4 × O_2(GC) mol × 100] /Q

Where O_2(GC) is the amount of generated oxygen gas determined by the GC and Q is the accumulated charge obtained from bulk electrolysis experiment.

Working Electrode Modification. A mixture of 2.5 mg of carbon black and 5 mg of the catalyst material was dispersed in 1.02 mL isopropanol and 4.08 µL Nafion solution. The resulting solution was sonicated for 30 minutes to form a homogeneous catalyst ink. Then 10 µL of the as-prepared catalysts ink was dropcasted on top of a glassy carbon electrode with a geometric area of 0.196 cm^2, which was cleaned by sonication in acetone, isopropyl alcohol, and water prior to use. Afterwards, the glassy carbon disk was rotated at a speed of 600 RPM to dry the ink suspension. The resultant catalyst loading on the glassy carbon disk electrode was 0.25 mg/cm^2.

RESULTS AND DISCUSSION

All the characterization and electrochemical studies were performed on dried ZrP samples. Since θ-ZrP transforms to α-ZrP after it is dehydrated, the physical and electrochemical properties of CoTcPP/ZrP will be compared to α-ZrP. The FT-IR spectra of α-ZrP, CoTcPP and CoTcPP/ZrP are presented in Figure 1. The pure α-ZrP sample shows the characteristic orthophosphate group vibrations at 962 and 1031 cm^{-1}, while

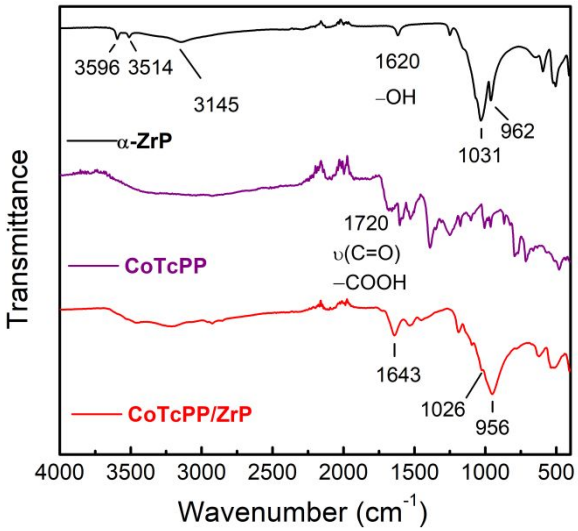

Figure 1. FT-IR spectra of (from top to bottom): α-ZrP, CoTcPP and CoTcPP/ZrP.

the bands observed at 3514 and 3596 cm^{-1} can be attributed to the water molecules inside the ZrP layers and the bands at 1620 and 3145 cm^{-1} are assigned to the –OH groups. These observations are consistent with previously reported studies.[47,48] The FT-IR spectrum of CoTcPP/ZrP is dominated by the peaks of ZrP with respect to the porphyrin signals. This is presumably due to the relative high concentration of ZrP in the sample and that some Co porphyrin molecules are embedded inside the layers. However, the relative intensity of the bands that belong to the water molecules decreases in CoTcPP/ZrP, implying partial water displacement inside ZrP layers by the CoTcPP molecule. In addition, several new peaks are observed at the region from 1500 to 1700 cm^{-1} in CoTcPP/ZrP, which are attributed to the typical C=C and C=N stretching of the porphyrin macrocycle. Furthermore, notable shifts of some of the peaks belonging to ZrP are observed in the CoTcPP/ZrP sample when comparing to the pristine α-ZrP. Specifically, the peaks for the orthophosphate groups in CoTcPP/ZrP are observed at 956 and 1026 cm^{-1} and the bending vibration for –OH group seen at 1620 cm^{-1} for ZrP exhibits a hypochromic shift (1643 cm^{-1} in CoTcPP/ZrP) after intercalation. Previous reports have shown that ZrP can immobilize carboxylic acids into its layers.[49,50] We hypothesize that the successful intercalation of this metalloporphyrin molecule in ZrP is similarly due to strong interactions between the carboxylate groups and ZrP which results in the orthophosphate IR shifts mentioned above. A proposed scheme of how the CoTcPP molecules are intercalated by ZrP is included in the Supporting Information. Moreover, the band at 1720 cm^{-1}, indicative of free carboxylic acid groups, has a lower intensity in CoTcPP/ZrP compared to the free molecule suggesting carboxylate-ZrP interactions. To further test this hypothesis, we tried the intercalation of carboxylate-free meso-tetraphenylporphyrin in ZrP under the

same conditions. Under these conditions we were not able to observe porphyrin intercalation. Thus, the carboxylic groups are essential for the
successful intercalation of the porphyrin molecule.

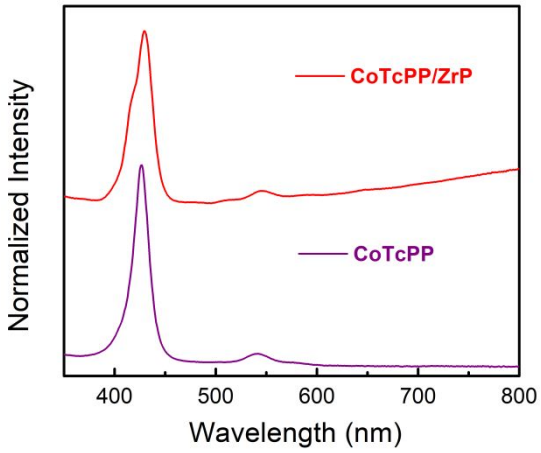

Figure 2. Overlaid UV-Vis spectra of CoTcPP in ethanol solution and CoTcPP/ZrP in ethanol suspension. The absorption spectrum of CoTcPP/ZrP was baseline corrected.

Figure 2 shows the overlaid UV-Vis spectra of CoTcPP in an ethanol solution and CoTcPP/ZrP in an ethanol suspension. CoTcPP exhibits an intense Soret band at 429 nm and a weak band at 546 nm in the Q band region. The absorption spectrum of CoTcPP/ZrP shows the same bands as the molecular CoTcPP which indicates the presence of the cobalt porphyrin molecule in CoTcPP/ZrP.

The cobalt porphyrin molecules can be surface bound to ZrP or intercalated between the layers. Surface-adsorbed molecular species are not supposed to change the interlayer distance in ZrP, while the insertion of molecules inside ZrP is expected to do so. This can be analyzed by X-ray powder diffraction (XRPD) measurements. The first diffraction peak of α-ZrP at 2θ = 11.5° (Figure 3) corresponds to the (002) Miller plane, and results in an interlayer distance of 7.6 Å. To compare, the XRPD patterns of CoTcPP/ZrP show a 2θ of 9.14° for the same (002) plane which corresponds to an interlayer distance of 9.58 Å. This

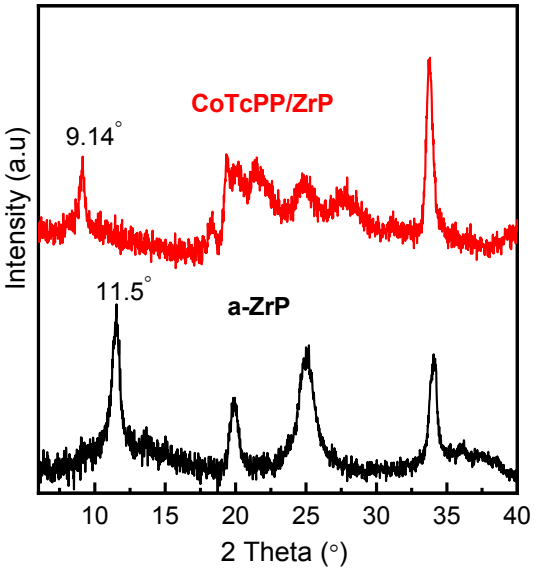

Figure 3. X-ray powder diffraction patterns of α-ZrP and CoTcPP/ZrP.

Figure 4. Overlaid XPS survey of CoTcPP/ZrP and α-ZrP.

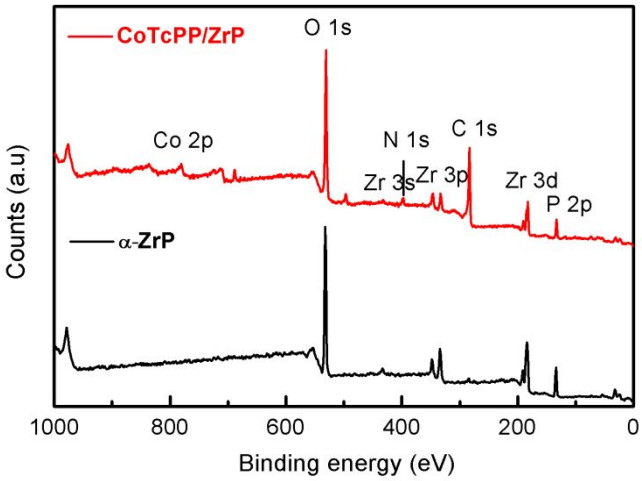

suggests that the (002) plane is expanded due to the intercalant species. The expanded interlayer distance is significantly smaller than the longest atom-to-atom distance within the porphyrin (*i.e.* from one carboxylic group to another opposite to it, c.a. 15 Å).[51,52] We suggest that the CoTcPP molecules may be partially embedded inside the ZrP layers. This is possible since the porphyrin molecules interact with ZrP through their carboxylate functional groups. Additionally, the diffraction peaks for (020) and $(31\bar{2})$ planes at 2θ ≈ 34° remain constant in both α-ZrP and CoTcPP/ZrP, suggesting the layered structure of ZrP is intact in CoTcPP/ZrP.[53] However, it is still possible that some of the CoTcPP molecules are surface-absorbed on the ZrP in addition to those embedded inside the layers.

Elemental mapping analyses, energy dispersive X-ray (EDX), and X-ray photoelectron spectroscopy (XPS) were performed in order to evaluate the elemental composition of α-ZrP and CoTcPP/ZrP. The elemental maps (Figure S3) and EDX spectrum (Figure S4) of α-ZrP confirm the presence of Zr, P and O. In comparison, CoTcPP/ZrP shows the presence of Co and C in addition to Zr, P and O, which is also corroborated by its elemental maps and EDX spectrum (Figure S5 and Figure S6 respectively). In addition, XPS survey scans (Figure 4) of CoTcPP/ZrP show the introduction of Co spectral lines further confirming the successful modification of ZrP with CoTcPP. Results obtained from inductively coupled plasma mass spectrometry (ICP-MS) analysis show a Co content of 3.38 wt% ± 0.37 wt% corresponding to an estimated molar ratio of 1 CoTcPP and 1.4 ZrP.

Cyclic voltammetry was conducted in 0.1 M KOH aqueous solution using the catalyst-modified glassy carbon working electrode (see Experimental Section) to evaluate the OER electrocatalytic performance of CoTcPP/ZrP and pristine α-ZrP modified with carbon black. All the samples studied in electrochemical studies were combined with carbon black to create a conductive surface since ZrP is known to exhibit poor electrical conductivity.[54] The cyclic voltammogram of CoTcPP/ZrP (Figure 5a) indicates that this material is

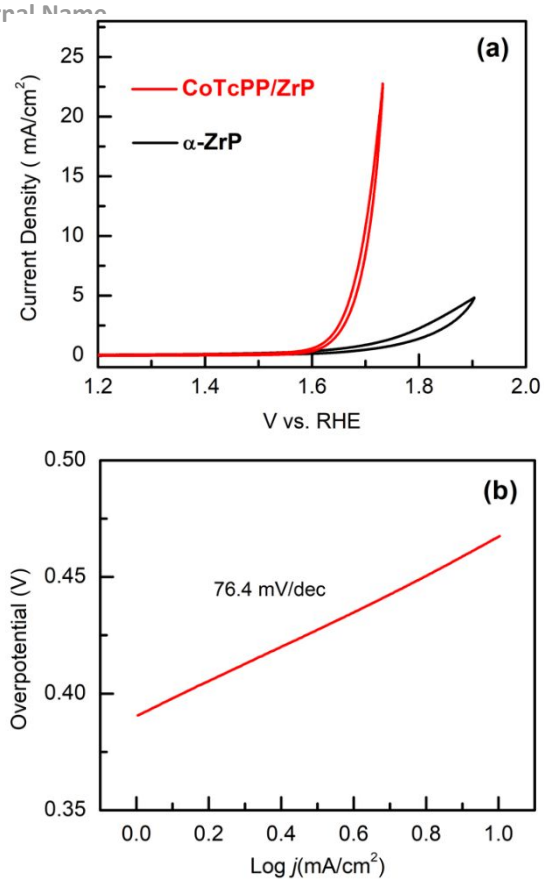

Figure 5. (a) Cyclic voltammograms of CoTcPP/ZrP and α-ZrP on a rotating disk electrode in 0.1 M KOH aqueous solutions. Scan rate: 10 mV/s. Both CoTcPP/ZrP and α-ZrP were modified with carbon black to enhance conductivity; (b) Tafel plot of CoTcPP/ZrP.

electrocatalytically active towards water oxidation, showing a modest overpotential (η) of 0.467 V at current density (j) of 10 mA/cm^2, while ZrP does not show considerable catalytic current at the studied potential range (black trace in Figure 5a). Electrodes coated with the pristine CoTcPP molecule and carbon black were also used as heterogeneous catalysts for OER studies. However, CoTcPP immediately dissolves into the electrolyte solution presumably due to its carboxylic groups. Thus, assessing the CoTcPP molecule as a heterogeneous electrocatalyst in basic media is challenging. This also suggests that CoTcPP is protected after intercalation into ZrP. While we cannot directly compare the electrocatalytic performance of CoTcPP/ZrP with the CoTcPP molecule, other Co porphyrin molecules with different substituents have been assessed as heterogeneous OER electrocatalysts in the literature.[55] These pristine Co porphyrin molecules generally exhibit an onset potential spanning between 1.71 V to 1.90 V vs. RHE in KOH solutions (see Table S1) and do not reach a 10 mA/cm^2 current density, while CoTcPP/ZrP shows an onset potential of around 1.61 V vs. RHE and a relatively fast increase in current density, indicating that molecular intercalation yields a material that is a more efficient OER electrocatalyst compared to molecular Co porphyrins. We have also combined the CoTcPP with ZrP and carbon black physically which are deposited on the glassy carbon electrode. The cyclic voltammogram of this mixture shows increase of anodic current with an onset potential of 1.62 V Vs. RHE that is comparable to CoTcPP/ZrP, albeit at significantly slower current density increase (η = 0.660 V at j = 10 mA/cm^2) (Figure S7) with respect to CoTcPP/ZrP.

Bulk electrolysis along with gas detection were performed at a constant potential of 1.9 V vs. RHE and the accumulated charge over 1 hour and 20 minutes is shown in Figure S8. The generated charge is found to be around 3.1 C while the amount of oxygen gas generated at the compartment of the cell containing the working electrode was determined to be 7.5 µmol, corresponding to a Faradaic efficiency of ca. 92% (see Experimental Section for the detailed calculation.

The Tafel plot of CoTcPP/ZrP is presented in Figure 5b and the Tafel slope is obtained from the equation: η = b × log(j) + a (where b is the Tafel slope and a is a constant). The catalyst CoTcPP/ZrP shows a Tafel slope of 76.4 mV/dec in 0.1 M KOH media suggesting fast OER reaction kinetics. The catalytic efficiency of this catalyst is comparable to its analogues catalytic systems, where transition metal cations (Fe^{2+}, Fe^{2+}, Ni^{2+}, Co^{2+}) are supported by different types of ZrP, and it is also comparable to some of the porphyrin-derived heterogeneous OER catalysts (Table S1). We have also performed long-term control-potential electrolysis using CoTcPP/ZrP in 0.1 M KOH solutions to evaluate the stability of the catalyst. Figure 6 shows that the current density decreases minimally over constant electrolysis of 65 hours demonstrating remarkable catalytic stability of CoTcPP/ZrP, which is essential for large-scale industrial application. The KOH electrolyte solution after the long-term electrolysis was subjected to UV-Vis spectroscopic measurement to see if there were CoTcPP molecules dissolved in the solution. As a result, the UV-Vis spectrum shows no evidence of the CoTcPP characteristic absorption (Figure S9), indicating that the CoTcPP molecules remain on the working electrode. The CoTcPP/ZrP was also characterized by UV-Vis spectroscopy after long-term bulk electrolysis in 0.1 M KOH to further investigate the stability of the catalyst. The UV-Vis

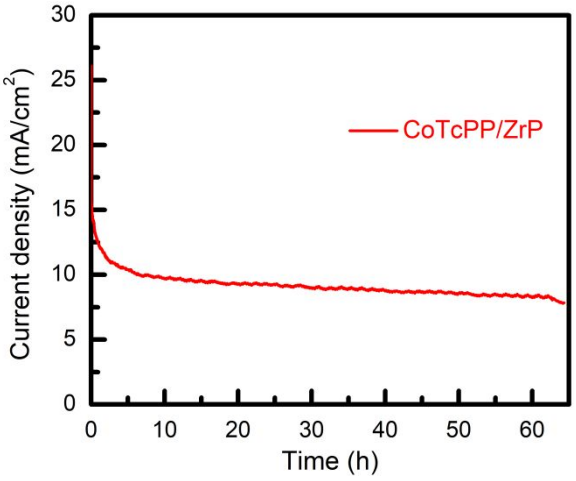

spectra of CoTcPP/ZrP combined with carbon black are identical

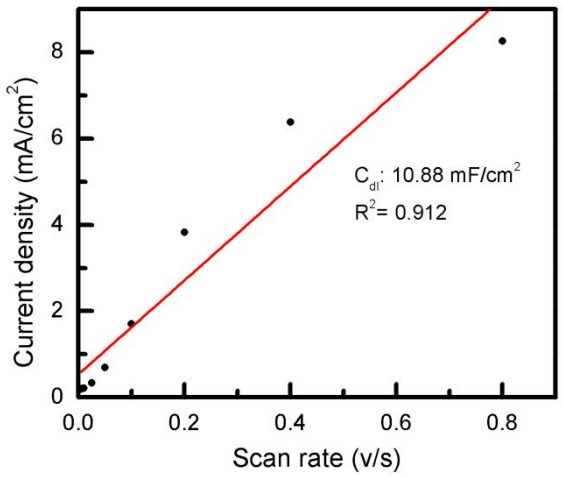

Figure 6. Control-potential bulk-electrolysis using CoTcPP/ZrP in 0.1 M KOH aqueous solution

Figure 7. Linear fit plots of scan rates as a function of double layer charging current for CoTcPP/ZrP in 1.0 M KOH. Scan rate: 0.005 V/s, 0.01 V/s, 0.025 V/s, 0.05 V/s, 0.1 V/s, 0.2 V/s, 0.4 V/s, 0.8 V/s.

before and after bulk electrolysis as shown in Figure S10, suggesting that the CoTcPP in this material is intact.

The electrochemically active surface area (EASA) of CoTcPP/ZrP is determined by carrying out parallel cyclic voltammetric experiments in the double-layer region with different scan rates in 0.1 M KOH solution. The dependence of current density on scan rate is plotted in Figure 7 and the overlaid cyclic voltammograms are included in Figure S8. An active surface area of 272 cm^2 is obtained by the equation: ECSA = C_{dl}/C_s, where the reported specific capacitance of 0.04 mF/cm^2 in KOH was used.[56,57]

The electronic properties of CoTcPP/ZrP under oxidation conditions were characterized by electrochemical impedance

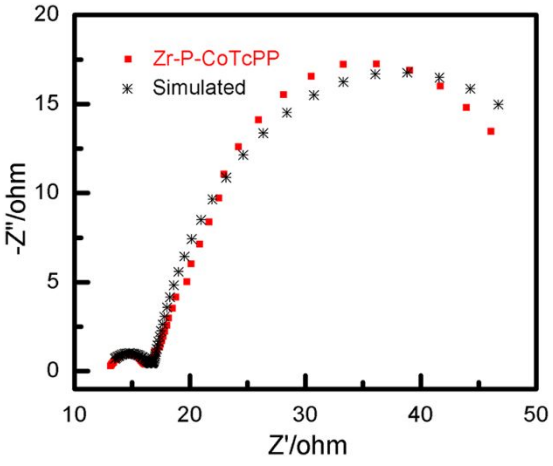

Figure 8. Electrochemical impedance spectroscopy and simulation fit spectra of the oxygen evolution reaction on the CoTcPP/ZrP electrode under oxidation condition in 0.1 M KOH aqueous solution.

spectroscopy (EIS) in order to study the interface charge transfer process. The Nyquist plots of CoTcPP/ZrP (Figure 8) at η = 0.250 V were obtained from the parallel combination of Faradaic charge transfer resistance and non-Faradaic double-layer capacitance. Two semicircular portions were obtained from the Nyquist plots at high and low frequencies corresponding to two electron-transfer limited processes and interpreted by using Randle's model with two parallel R||C circuits in series where the current must first pass through the ZrP layers before reaching the electrocatalytic active species. Under oxidation conditions, the Randle's model is in good agreement with the experimental data. The simulated model consists of electrolyte resistance (Rs), electron-transfer resistance generated from ZrP layers (R1) and the double layer capacitance (CPE1), electron-transfer resistance arising from ZrP layers with CoTcPP (R2) and its corresponding double layer capacitance (CPE2). The value of R2 (42.31 ohm) is significantly higher than those of Rs and R1 (12.62 ohm and 4.28 ohm, respectively) indicating that the layers containing the CoTcPP limit the electron-transfer process during oxidation, suggesting the electrocatalysis occurs through the porphyrin centers.

Conclusions

We have shown in this study the use of ZrP as a layered catalyst support for a cobalt porphyrin molecule to construct a metalloporphyrin-derived heterogeneous electrocatalyst. The cobalt porphyrin molecule has shown to be successfully intercalated into ZrP layers which is evidenced by various standard physical characterization and is able to electrochemically produce oxygen gas from basic aqueous solution with impressive catalytic durability. These findings may expand the use of ZrP as supporting platforms for a more variety of molecular catalysts in addition to ionic metals and provide alternative approaches to heterogenize porphyrin-based catalytic systems.

Conflicts of interest

There are no conflicts to declare.

Acknowledgements

This work was funded by NSF under award number CHE-1305124, and by ONR under award number ONR N00014-19-1-2467. IBA was supported by the Undergraduate Biomedical Research Training at UTEP/MARC, grant number 2T34GM008048, and by the Summer Research – Early Identification Program (SR-EIP) at Stanford University. MVRG was supported by the National Science Foundation under the NSF Center for Chemical Innovation in Solar Fuels CHE-1305124 and the NSF-PREM Center for Interfacial Electrochemistry of

Energy Materials (CiE2M) grant DMR-1827622. The authors acknowledge that part of this work was performed at the Stanford Nano Shared Facilities (SNSF), supported by the National Science Foundation under award ECCS-1542152.

Notes and references

1 A. K. Rohit, Ksh. P. Devi and S. Rangnekar, *J. Energy Storage*, 2017, **13**, 10–23.
2 T. R. Cook, D. K. Dogutan, S. Y. Reece, Y. Surendranath, T. S. Teets and D. G. Nocera, *Chem. Rev.*, 2010, **110**, 6474–6502.
3 J. A. Turner, *Science*, 2004, **305**, 972–974.
4 N. S. Lewis and D. G. Nocera, *Proc. Natl. Acad. Sci.*, 2006, **103**, 15729–15735.
5 L. G. Bloor, R. Solarska, K. Bienkowski, P. J. Kulesza, J. Augustynski, M. D. Symes and L. Cronin, *J. Am. Chem. Soc.*, 2016, **138**, 6707–6710.
6 M. G. Walter, E. L. Warren, J. R. McKone, S. W. Boettcher, Q. Mi, E. A. Santori and N. S. Lewis, *Chem. Rev.*, 2010, **110**, 6446–6473.
7 C. Costentin and D. G. Nocera, *Proc. Natl. Acad. Sci.*, 2017, **114**, 13380–13384.
8 H. Chen, Z. Sun, X. Liu, A. Han and P. Du, *J. Phys. Chem. C*, 2015, **119**, 8998–9004.
9 D. K. Zhong and D. R. Gamelin, *J. Am. Chem. Soc.*, 2010, **132**, 4202–4207.
10 M. Gong, Y. Li, H. Wang, Y. Liang, J. Z. Wu, J. Zhou, J. Wang, T. Regier, F. Wei and H. Dai, *J. Am. Chem. Soc.*, 2013, **135**, 8452–8455.
11 I. Bhugun, D. Lexa and J.-M. Savéant, *J. Am. Chem. Soc.*, 1996, **118**, 3982–3983.
12 D. K. Bediako, B. H. Solis, D. K. Dogutan, M. M. Roubelakis, A. G. Maher, C. H. Lee, M. B. Chambers, S. Hammes-Schiffer and D. G. Nocera, *Proc. Natl. Acad. Sci.*, 2014, **111**, 15001–15006.
13 B. B. Beyene, S. B. Mane and C.-H. Hung, *J. Electrochem. Soc.*, 2018, **165**, H481–H487.
14 Y. Han, Y. Wu, W. Lai and R. Cao, *Inorg. Chem.*, 2015, **54**, 5604–5613.
15 R. M. Kellett and T. G. Spiro, *Inorg. Chem.*, 1985, **24**, 2373–2377.
16 T. Nakazono, A. R. Parent and K. Sakai, *Chem. Commun.*, 2013, **49**, 6325–6327.
17 B. B. Beyene, S. B. Mane and C.-H. Hung, *Chem. Commun.*, 2015, **51**, 15067–15070.
18 Y. Liu, Y. Han, Z. Zhang, W. Zhang, W. Lai, Y. Wang and R. Cao, *Chem. Sci.*, 2019, **10**, 2613–2622.
19 X. Wang, Z.-F. Cai, D. Wang and L.-J. Wan, *J. Am. Chem. Soc.*, 2019, **141**, 7665–7669.
20 S. Yamazaki, *Coord. Chem. Rev.*, 2018, **373**, 148–166.
21 H. Jia, Y. Yao, Y. Gao, D. Lu and P. Du, *Chem. Commun.*, 2016, **52**, 13483–13486.
22 S. Cui, M. Qian, X. Liu, Z. Sun and P. Du, *ChemSusChem*, 2016, **9**, 2365–2373.
23 Y. Wu, J. M. Veleta, D. Tang, A. D. Price, C. E. Botez and D. Villagrán, *Dalton Trans.*, 2018, **47**, 8801–8806.
24 A. Han, H. Jia, H. Ma, S. Ye, H. Wu, H. Lei, Y. Han, R. Cao and P. Du, *Phys. Chem. Chem. Phys.*, 2014, **16**, 11224–11232.
25 A. V. Marín, M. J. Aguirre, J. Muena, W. Dehaen, W. Maes, H. T. Ngo, G. Ramírez and M. C. Arévalo, *Int. J. Electrochem. Sci.*, 2014, **10**, 3949–3960.
26 H. Tang, H. Yin, J. Wang, N. Yang, D. Wang and Z. Tang, *Angew. Chem. Int. Ed.*, 2013, **52**, 5585–5589.
27 G. S. Machado, P. B. Groszewicz, K. A. D. de F. Castro, F. Wypych and S. Nakagaki, *J. Colloid Interface Sci.*, 2012, **374**, 278–286.
28 J. Choi, P. Wagner, R. Jalili, J. Kim, D. R. MacFarlane, G. G. Wallace and D. L. Officer, *Adv. Energy Mater.*, 2018, **8**, 1801280.
29 I. Hod, M. D. Sampson, P. Deria, C. P. Kubiak, O. K. Farha and J. T. Hupp, *ACS Catal.*, 2015, **5**, 6302–6309.
30 N. Zhang, L. Wang, H. Wang, R. Cao, J. Wang, F. Bai and H. Fan, *Nano Lett.*, 2018, **18**, 560–566.
31 F. Bellezza, A. Cipiciani, U. Costantino and M. E. Negozio, *Langmuir*, 2002, **18**, 8737–8742.
32 J. F. Callejas, C. G. Read, C. W. Roske, N. S. Lewis and R. E. Schaak, *Chem. Mater.*, 2016, **28**, 6017–6044.
33 J. M. Troup and A. Clearfield, *Inorg. Chem.*, 1977, **16**, 3311–3314.
34 G. Alberti, U. Costantino and J. S. Gill, *J. Inorg. Nucl. Chem.*, 1976, **38**, 1733–1738.
35 A. A. Martí and J. L. Colón, *Inorg. Chem.*, 2003, **42**, 2830–2832.
36 J. Sanchez, M. V. Ramos-Garcés, I. Narkeviciute, J. L. Colón and T. F. Jaramillo, *Catalysts*, 2017, **7**, 132.
37 K. N. Rao, A. Sridhar, A. F. Lee, S. J. Tavener, N. A. Young and K. Wilson, *Green Chem.*, 2006, **8**, 790–797.
38 M. Tang, T. Yang and Y. Zhang, *Sci. China Technol. Sci.*, 2016, **59**, 436–441.
39 A. Díaz, M. L. González, R. J. Pérez, A. David, A. Mukherjee, A. Báez, A. Clearfield and J. L. Colón, *Nanoscale*, 2013, **5**, 11456–11463.
40 M. B. Santiago, C. Declet-Flores, A. Díaz, M. M. Vélez, M. Z. Bosques, Y. Sanakis and J. L. Colón, *Langmuir*, 2007, **23**, 7810–7817.
41 M. V. Ramos-Garcés, J. Sanchez, D. E. Del Toro-Pedrosa, I. B. Alvarez, Y. Wu, E. Valle, D. Villagrán, T. F. Jaramillo and J. L. Colón, *ACS Appl. Energy Mater.*, 2019, **2**, 3561–3567.

42 M. V. Ramos-Garcés, J. Sanchez, K. L. Luz-Rivera, D. E. D. Toro-Pedrosa, T. F. Jaramillo and J. L. Colón, *Dalton Trans.*, 2020, **49**, 3892–3900.
43 M. V. Ramos-Garcés, J. Sanchez, I. B. Alvarez, Y. Wu, D. Villagrán, T. F. Jaramillo and J. L. Colón, *Water Chem.*, 2019.
44 B. Casañas-Montes, A. Díaz, C. Barbosa, C. Ramos, C. Collazo, E. Meléndez, C. Queffelec, F. Fayon, A. Clearfield, B. Bujoli and J. L. Colón, *J. Organomet. Chem.*, 2015, **791**, 34–40.
45 T. Kijima, *Bull. Chem. Soc. Jpn.*, 1982, **55**, 3031–3032.
46 H. Shahroosvand, S. Zakavi, A. Sousaraei, E. Mohajerani and M. Mahmoudi, *Dalton Trans.*, 2015, **44**, 8364–8368.
47 Y. Zhou, R. Huang, F. Ding, A. D. Brittain, J. Liu, M. Zhang, M. Xiao, Y. Meng and L. Sun, *ACS Appl. Mater. Interfaces*, 2014, **6**, 7417–7425.
48 S. E. Horsley, D. V. Nowell and D. T. Stewart, *Spectrochim. Acta Part Mol. Spectrosc.*, 1974, **30**, 535–541.
49 M. Mazur, P. Krysiński and G. J. Blanchard, *Langmuir*, 2005, **21**, 8802–8808.
50 S. B. Bakiamoh and G. J. Blanchard, *Langmuir*, 2001, **17**, 3438–3446.
51 Q. Yuan, Y. Xing and E. Borguet, *J. Am. Chem. Soc.*, 2010, **132**, 5054–5060.
52 Y. Diskin-Posner and I. Goldberg, *Chem. Commun.*, 1999, 1961–1962.
53 A. Díaz, V. Saxena, J. González, A. David, B. Casañas, C. Carpenter, J. D. Batteas, J. L. Colón, A. Clearfield and M. D. Hussain, *Chem. Commun. Camb. Engl.*, 2012, **48**, 1754–1756.
54 Y. Liu, W. Yan, W. Zhang, W. Kong, Z. Wang, X. Hao and G. Guan, *ChemSusChem*, 2019, **12**, 5172–5182.
55 N. Morlanés, K. S. Joya, K. Takanabe and V. Rodionov, *Eur. J. Inorg. Chem.*, 2015, **2015**, 49–52.
56 C. C. L. McCrory, S. Jung, J. C. Peters and T. F. Jaramillo, *J. Am. Chem. Soc.*, 2013, **135**, 16977–16987.
57 S. Iseki, K. Ohashi and S. Nagaura, *Electrochimica Acta*, 1972, **17**, 2249–2265.

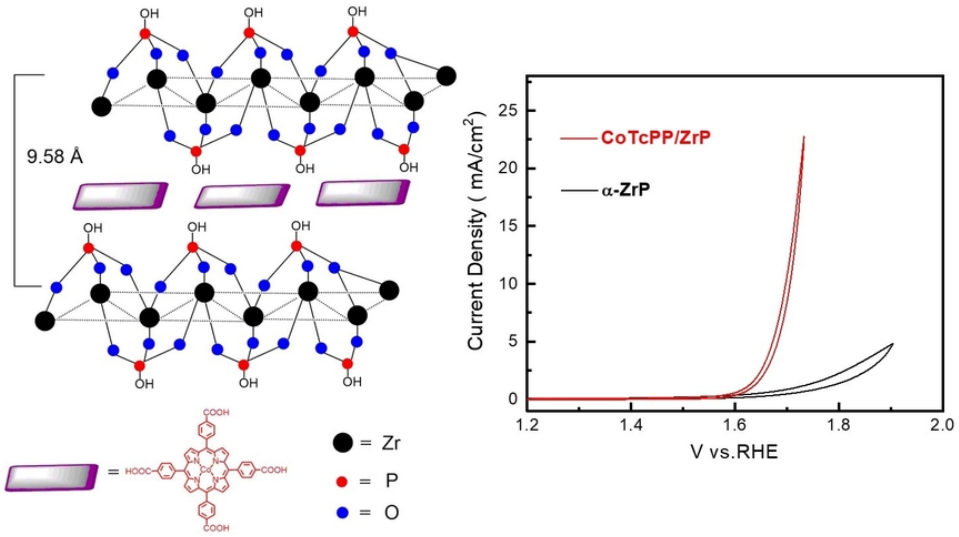

76x40mm (300 x 300 DPI)